The IR, Raman and Microwave Spectra and the Molecular Structure of 1,4-Difluoro-2-butyne

A. Karlsson, P. Klæboe*, K.-M. Marstokk, H. Møllendal* and C. J. Nielsen

Department of Chemistry, University of Oslo, N-0315 Oslo 3, Norway

Karlsson, A., Klæboe, P., Marstokk, K.-M., Møllendal, H. and Nielsen, C. J., 1986. The IR, Raman and Microwave Spectra and the Molecular Structure of 1,4-Difluoro-2-butyne. – Acta Chem. Scand. A 40: 374–386.

The IR spectra of 1,4-difluoro-2-butyne (DFB) as a vapour, liquid and crystalline solid at 90 K and as a high pressure crystal were recorded in the 4000–40 cm^{-1} range. Spectra of DFB isolated in argon and nitrogen matrices were studied to 200 cm^{-1}. Raman spectra of the liquid and of the crystalline solid were recorded and semiquantitative polarization data obtained. The microwave spectrum was investigated extensively in the 12.4–22.0 GHz spectral region, but measurements were also made in the upper *K*- and *R*-bands. Unlike the dichloro- and dibromo-compounds, DFB does not exhibit free or nearly free internal rotation but is present as only one conformer – *gauche* – in all states of aggregation, as well as in the argon and nitrogen matrices. Consequently, all the fundamental modes of vibration have been assigned in terms of C_2 symmetry in good agreement with the results of a normal coordinate calculation. Microwave spectra of two vibrationally excited states were assigned; the more intense corresponding to the torsional mode at 42(5) cm^{-1}; the other to the second lowest skeletal bending vibration at 188(40) cm^{-1}. Most transitions of the torsionally excited state were split, presumably due to tunnelling through a low barrier. The dihedral angle was found to be 99(3)° from *syn*. The potential function for the torsion was determined assuming that terms higher than V_2 in the Taylor expansion can be neglected. The two first potential constants were found to be $V_1 = -1.9$ kJ mol^{-1} and $V_2 = -3.1(7)$ kJ mol^{-1}, yielding the barriers at *syn* and *anti* as 4.1(10) kJ mol^{-1} and 2.2(5) kJ mol^{-1}, respectively. Extensive centrifugal distortion analyses were carried out for the ground and the vibrationally excited states.

The 1,4-dihalo-2-butynes are interesting compounds from a conformational viewpoint since the barrier to internal rotation is much lower than for the corresponding 1,2-dihaloethanes. Hence, in addition to the staggered conformations, *anti* and *gauche*, the 1,4-dihalo-2-butynes exhibit large torsional amplitudes or even essentially free internal rotation.

Various papers dealing with the vibrational spectra[1–8] and electron diffraction results[9,10] of 1,4-dichloro- and 1,4-dibromo-2-butyne have been reported. However, even for 1,4-dichloro-2-butyne, studied in considerable detail, the conformers present in the liquid and crystalline stated[4,6,8] are not well understood. For 1,4-difluoro-2-butyne (DFB) an *ab initio* molecular orbital calculation (4-31G basis set) has been published[11] suggesting a stable conformation around 100° from *syn*; but no experimental results are known except for a few mid IR frequencies.[2] It was therefore decided to make new comprehensive spectroscopy studies of DFB. Our results for DFB will be presented here; the conclusions regarding 1,4-dichloro-2-butyne will be published shortly.[12]

Experimental

Preparation. The preparation of DFB has previously been described.[13] However, the experimental conditions were not given in detail. Our procedure, which gave a higher yield, is briefly outlined below.

DFB was prepared by heating KF (2.93 mol)

*To whom correspondence should be addressed.

with 1 dm^3 diethyleneglycol to 120 °C at 175 torr and adding 1,4-dichloro-2-butyne with stirring. The DFB formed was collected in a trap kept at dry ice temperature. The product contained DFB, 1-fluoro-4-chloro-2-butyne and unreacted 1,4-dichloro-2-butyne. A coarse separation was performed in a Rotaband® column and the final purification by preparative GC on an Apiezon® column. Purity >99 %, b.p. 45 °C/150 torr, yield ca. 3 %.

Instrumental. The IR spectra were recorded with a Perkin-Elmer model 225 (4000–200 cm^{-1}) and a Bruker FTIR model 114C evacuable spectrometer (4000–20 cm^{-1}). Vapour cells with 20 and 10 cm path lengths had windows of CsI and polyethylene, respectively; the sealed liquid cells had windows of KBr, CsI, AgCl and polyethylene. Cryostats with CsI and silicon windows were used at liquid nitrogen temperature. Spectra of DFB isolated in argon and nitrogen matrices (S/M = 1:700) were recorded at 13 K using a closed cycle cryostat (Air Products) equipped with CsI windows. High pressure spectra were recorded with a diamond anvil cell (DAC) with type IIa diamonds, combined with a Perkin-Elmer 4× beam condensor.

Raman spectra were obtained with a Dilor model RT30 spectrometer (triple monochromator) interfaced with the Aspect® 2000 computer of the Bruker spectrometer. An argon ion laser (CRL 52G) in the 90° and 180° scattering geometry and the lines 514.5 and 488.0 nm were employed for excitation. Semiquantitative polarization measurements were obtained of the neat liquid, while amorphous and annealed crystalline deposits on a cooled copper finger were studied at 90 K.

The microwave spectrum was investigated extensively in the 12.4–22.0 GHz spectral region. Many measurements were also made in the upper *K*- and *R*-bands. The experiments were made with the cell cooled to about −40 °C and a pressure of roughly 1 Pa. Lower temperatures could not be used due to insufficient vapour pressure of the compound. A conventional spectrometer with free-running clystrons was used.

Results

Vibrational spectra. The IR spectra of DFB in the vapour and liquid states are given in Figs. 1 and 2, respectively, whereas the low temperature spectra are shown in Figs. 3 (mid IR) and 4 (far IR). A high pressure spectrum of crystalline DFB at ca. 20 kbar is demonstrated in Fig. 5. A Raman spectrum of the liquid is shown in Fig. 6, while the crystalline and amorphous/crystalline spectra are given in Figs. 7 and 8. The observed IR and Raman spectral data are collected in Table 1.

Conformations. As is apparent from Figs. 1–8 and the data of Table 1, the IR and Raman spectra of the vapour, liquid and crystalline states are very similar. In particular, none of the bands present in the gaseous, liquid, and amorphous states vanished in the crystal spectra, strongly indicating that only one conformer was present in the various states of aggregation. The number of IR and Raman bands, which is surprisingly small, agrees with a one conformational preference in DFB in strong contradiction to the corresponding dichloro-[1,4,6–8,12] and dibromo- compounds.[5]

The principal moments of inertia around the *b*

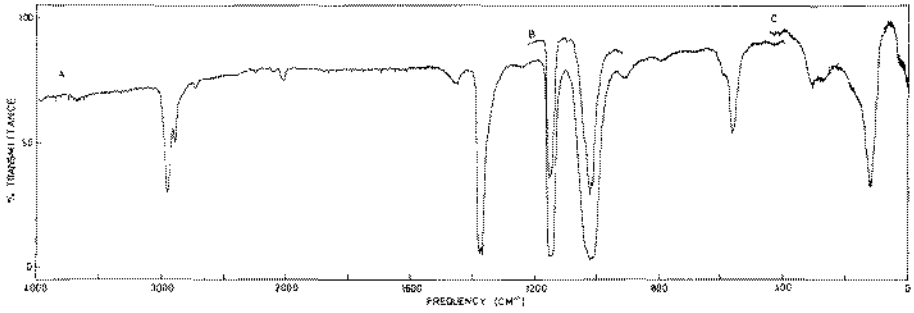

Fig. 1. IR spectrum of 1,4-difluoro-2-butyne as a vapour. A: 10 cm pathlength, 23 mm Hg; B: 10 cm pathlength, 5 mm Hg; C: 19 cm pathlength, 30 mm Hg.

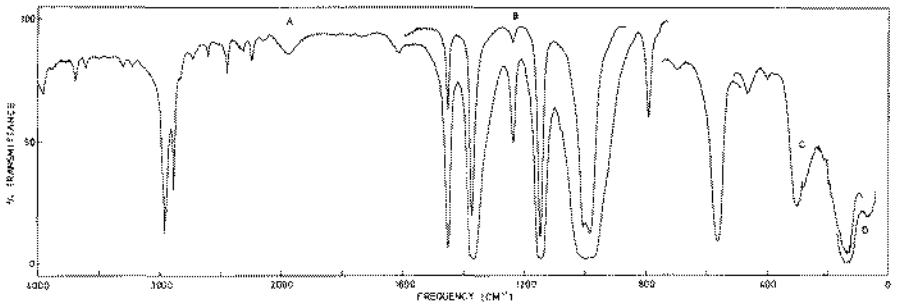

Fig. 2. IR spectrum of 1,4-difluoro-2-butyne in the liquid phase. A: 0.05 mm; B: thin film; C,D: 25 % cyclohexane solution, 1 mm.

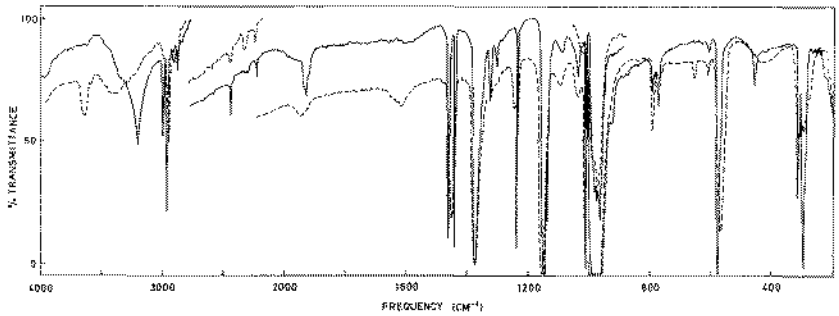

Fig. 3. IR spectrum of 1,4-difluoro-2- butyne as a crystalline solid (——) and as an amorphous solid (– – –).

and *c* axes are nearly 10 times larger than around the *a* axis leading to a nearly prolate rotor. Only minor variations in the IR vapour phase band contours with the dihedral angle are expected, making the IR vapour spectrum of little help in deciding the molecular symmetry. Moreover, the observed vapour contours (Fig. 1) are ill defined, probably as a result of prominent hot band transitions connected with the low frequency torsional mode.

Besides having free or nearly free internal rotation (D_2*)[34], DFB can, in principle, exist in *syn* (C_{2v}), *gauche* (C_2) and *anti* (C_{2h}) conformations. From the normal band widths below 600 cm^{-1}

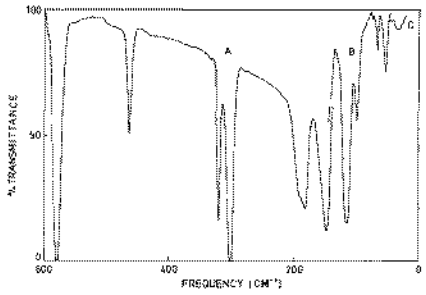

Fig. 4. FIR spectrum of 1,4-difluoro-2-butyne as a crystalline solid. Mylar beam splitter. A: 3.5 μ, B: 12 μ, C: 23 μ.

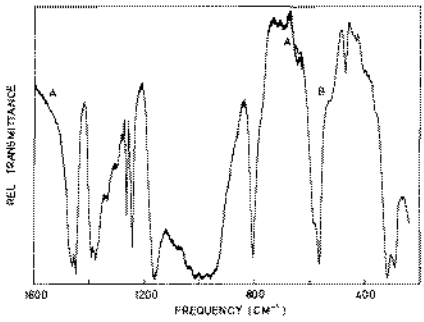

Fig. 5. IR spectrum of 1,4-difluoro-2-butyne as a crystalline solid at ca. 20 kbar. A: KBr beam splitter; B: 3.5 μ mylar beam splitter.

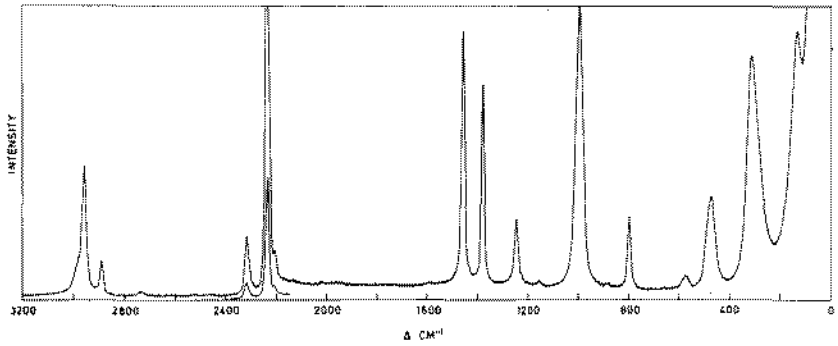

Fig. 6. Raman spectrum of 1,4- difluoro-2-butyne as a neat liquid.

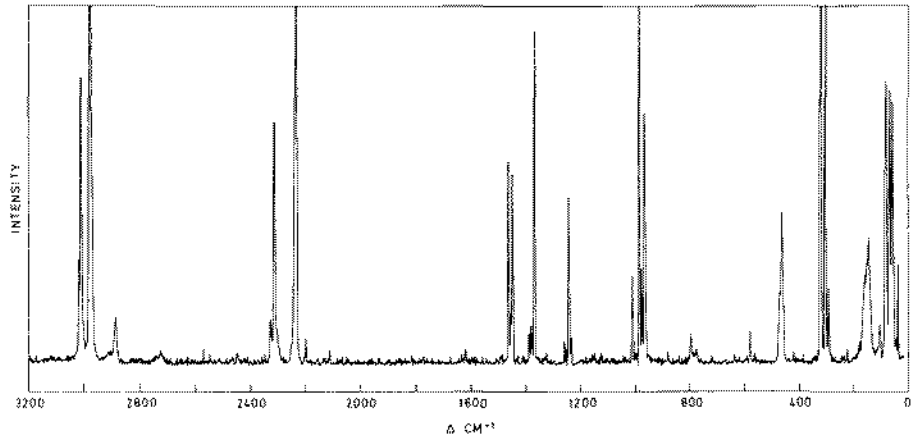

Fig. 7. Raman spectrum of 1,4-difluoro-2-butyne as a crystalline solid.

and from the lack of spectral variation from phase to phase, we have already excluded the possibility of free or nearly free internal rotation.

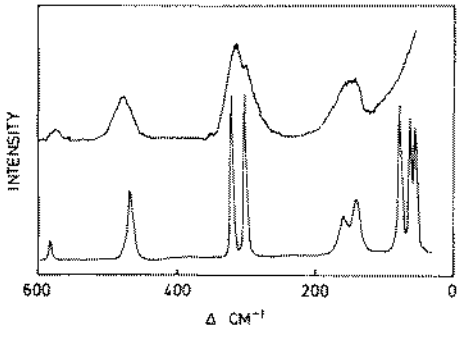

Fig. 8. Raman spectrum of 1,4-difluoro-2-butyne as an amorphous solid (A) and as a crystalline solid (B).

An *anti* conformation with C_{2h} symmetry can be ruled out immediately since nearly all the IR bands have Raman counterparts and vice versa. In the *syn* conformation (C_{2v}), we have an eclipsed structure with the FCCCCF skeleton lying in a plane. However, C_{2v} symmetry would require that the C-C≡C-C out-of-plane bending modes and the torsion should belong to species a_2 (IR inactive, R active) contrary to our results.

Unlike 1,4-dichloro-2-butyne, in which all the liquid bands below 700 cm^{-1} were very broad but sharpening in the low temperature spectra and believed to have "nearly free rotation",[1,9,12] the spectra indicated a higher barrier in DFB. Therefore, the vibrational spectra suggest that the *gauche* conformer (C_2) is present for DFB in all the phases: vapour, liquid, solution, amorphous, low temperature and high pressure crystalline

Table 1. Infrared and Raman spectral data for 1,4-difluoro-2-butyne.[a]

IR				Raman		Assignments
Ar-matrix	Vapour	Liquid	Cryst. (90K)	Liquid	Cryst. (90K)	
			3014 vw[g]		3017 s	
2974 m		~2980 w,sh		~2980 m,sh		ν_1 *a*, ν_{14} *b*
			3007 w		3010 vs	
	2964					
2957 s	m	2957 s	2977 m	2958 s,P	2978 vs	ν_2 *a*, ν_{15} *b*
	2958					
			2916 vw,br			comb.
	2904		2888 w			
2889 m	m	2880 m		2883 m,P	2886 m	$2\nu_4$, $2\nu_{16}$ *A*
	2894		2883 w			
	2830 w,sh	2828 w	2846 vw			comb.
				2238 vs,P		$\nu_4+\nu_9$, A Fr
~2240 vw	~2250 vw	~2235 w	2234 vw	2233 vvs,P	2236 vvs	ν_3 *a*
				2205 m,sh,P	2200 m	^{13}C
1456 m			1465 s		1462 s	
	~1460 w	1455 s		1456 vs,P?		ν_4 *a*, ν_{16} *B*
1454 m			1445 s		1447 s	
			1382 w,sh		1382 vw	
	1383					
1376 vs			1377 s		1379 m	
	1379 Q	vs 1375 vs		1378 vs,P?		ν_5 *a*, ν_{18} *b*
1374 s,sh			1370 s,sh		1369 vs	
	1374					
1362 m			1355 w,sh			
			1328 w			
			1306 vw			
			1248 vw			
1249 w			1243 mw		1244 m	
	~1240 w	1240 m		1242 m,br,P		ν_6 *a*, ν_{18} *b*
1239 w			1239 s		1240 m	
	1156					
1162 vs	vs	1154 vs	1147 vs,br	1154 vw,D	1149 vw	ν_{19} *b*
	1149					
			1141 m			
			1138 m			
		1089 w,sh				$\nu_9+\nu_{23}$ *B*
~1040 w			1041 w			comb.
1029 vvs	1042					
1025 s	1037					
	vs	1008 vs	1013 vs	~1005 vs,P?	1012 s	ν_7 *a*, ν_{20} *b*
1011 vvs	1033 Q					
1007 vs	1024		982 vs		986 vvs	
1004 s	1016	vs 986 vs	976 vs	~985 vs,P?		ν_8 *a*, ν_{21} *b*
1000 m			965 vs		967 s	
		~950 m,sh	953 m,sh		953 vvw	comb.
	~910 w	~925 w,sh	928 w,sh			

(contd. next page)

Table 1. (contd.)

IR				Raman		Assignments
Ar-matrix	Vapour	Liquid	Cryst. (90K)	Liquid	Cryst. (90K)	
			878 vw	872 vw,D?	~880 vw	$\nu_{10}+\nu_{22}$ *B*
795 w	790 w	794 m	793 w	794 m,P	795 w	ν_9 *a*
		~765 w	774 w		777 vw	$\nu_{10}+\nu_{23}$ *B*
		698 w				
	598 vw		594 vw,sh			comb.
573 s	567					
	m	564 s	580 s	~570 w,D	580 w	ν_{22} *b*
563 m	565					
		~470 w	464 w	473 m,br,P	464 s	ν_{19} *A*
304 w						
	~305 mw		319 s		319 vs	
301 m		~300 m,br		315 vs,br,D		ν_{11} *a*, ν_{23} *b*
	~265 mw,br		301 s		301 vs	
~285 vw						
			191 s,sh			
	~175 mw,sh					
			181 s			
					160 m	ν_{12} *a*, ν_{24} *b*
	~121 s	*~135 s,br*	*148 m*	*135 s,br,D*	*142 m*	
			115 m			
			99 w			*lattice*
					83 vs	*lattice*
			65 w		*67 vs*	*lattice*
	~35 s,br	*~55 w*				ν_{13} *a*
			52 w		58 vs	lattice

[a]Bands in the regions 2800–2300 and 2200–1500 cm^{-1} have been omitted.
[b]Abbreviations: s, strong; m, medium; w, weak; v, very; sh, shoulder; br, broad; P, polarized; D, depolarized; FR, Fermi resonance, ^{13}C: C≡C str. with a ^{13}C isotope.
[c]The region 300–30 cm^{-1} is recorded in cyclohexane solution.

solid. Finally, a *gauche* conformer was also determined in the microwave investigation, revealing a dihedral angle of 99(3)° in the vapour (see below) – in exceptionally good agreement with the *ab initio* calculations.[11] It may be noted, though it is certainly not so convincing, that the force constant calculations also indicate a dihedral angle around 100°.

Spectral interpretations. With C_2 symmetry, the IR and Raman spectra divide into 13 modes of species *a* and 11 of species *b*, which can be distinguished by the Raman polarization measurements. A normal coordinate analysis was also carried out by transferring the force constants employed by Lichene *et al.*[2,3] on 1,4-dihalo-2-butynes. Additional support for the interpretations is given by the data for 1-fluoro-2-propyne,[15] 2-butyne,[16], 2,4-hexadiyne,[17], 1,4-dichloro-2-butyne[1,4,6–8,12] and 1,4-dibromo-2-butyne.[5] The stretching vibrations in the carbon chain of DFB lie within 20 cm^{-1} from those of 2-butyne[16] and 1,4-dichloro-2-butyne.[12] Furthermore, the CH_2F vibrations nearly coincide with those of 1-fluoro-2-propyne[15] and appear as typical group frequencies. The six FCCCCF skeletal deformation modes (3*a* + 3*b*) are, however, delocalized, and the assignments heavily depend upon the results of the force constant calculations. Our assigned fundamentals are listed in Table 2 together with an approximate description according to the largest contribution to the potential energy distribution (PED).

It is immediately seen from Figs. 1–8 that DFB

Table 2. Observed and calculated[a] fundamental frequencies of vibration and centrifugal distortion constants.

No.	Observed[b]	Calculated	Approx. description
ν_1	2980	2978	CH_2 a.sym. str.
ν_2	2957	2946	CH_2 sym. str.
ν_3	2233[c]	2231	C≡C str.
ν_4	1455	1454	CH_2 scissor
ν_5	1375	1389	CH_2 wag
ν_6	1240	1237	CH_2 twist
ν_7	1008	1024	CH_2 rock
ν_8	986	998	C-F str.
ν_9	794	801	C-C str.
ν_{10}	474	477	skeletal def.
ν_{11}	300	292	skeletal def.
ν_{12}	135	125	skeletal def.
ν_{13}	−35	42	torsion
ν_{14}	2980	2978	CH_2 a.sym. str.
ν_{15}	2957	2946	CH_2 sym. str.
ν_{16}	1455	1455	CH_2 scissor
ν_{17}	1375	1389	CH_2 wag
ν_{18}	1240	1236	CH_2 twist
ν_{19}	1154	1147	C-C a.sym. str.
ν_{20}	1008	1023	CH_2 rock
ν_{21}	986	989	C-F a-sym. str.
ν_{22}	564	525	skeletal def.
ν_{23}	300	341	skeletal def.
ν_{24}	135	125	skeletal def.
τ_{aaaa}	−2.388[d]	−2.413	
τ_{bbbb}	−1.686	−1.684	
τ_{cccc}	−0.695	−0.678	
D_4	−42.4	−43.9	
D_5	0.147	0.139	

[a]Force field from Ref. 3.
[b]Infrared liquid phase values except when noted.
[c]Raman liquid phase value.
[d]For definition of the distortion constants, see Ref. 24. τ_{aaaa}, τ_{bbbb} and τ_{cccc} in MHz; D_4 and D_5 in kHz.

has very few IR and Raman bands compared to the 24 fundamentals expected. Apparently, the CH_2F stretching and bending modes have neglible mechanical coupling across the C-C≡C-C framework. Consequently, the in-phase motions of species *a* and the out-of-phase motions (*b*) overlap throughout the spectrum. Only in the argon and nitrogen matrices, can the *a* and *b* modes be observed as separate lines, frequently one or a few cm^{-1} apart. Since the IR spectra obtained in the argon and nitrogen matrices are very similar, the lines can be confidently ascribed to *a* and *b* modes rather than to matrix effects.

Large splittings were observed in the IR and Raman spectra of the crystal recorded at ca. 90 K, due to site and/or correlation effects. Certain strong IR and Raman bands below 300 cm^{-1} were detected in the crystal spectra only, and are undoubtedly lattice modes. The high pressure (ca. 17 kbar) IR crystal spectrum is similar to the low temperature spectrum, taking the lower resolution into consideration. A shift of most bands towards higher frequencies in the high pressure spectrum is generally observed.[18] It seems likely that the low temperature and high pressure crystals of DFB have the same lattice.

Microwave spectrum and assignment of the ground vibrational state. The microwave spectrum of 1,4-difluoro-2-butyne is very dense with absorptions occurring every few megahertz. It is also rather strong. The strongest lines turned out to be the ground state, $J_{2,J-2} \leftarrow J_{1,J-1}$ *b*-type *Q*-branch series with *J* between about 40 and 70 which have peak absorption coefficients of roughly 1×10^{-6} cm^{-1}. Assignment of the spectrum was made in the following manner. Model rotational constants were calculated for selected values of the F-C-C≡C-C-F dihedral angle using bond angles and distances taken from recent, accurate studies of related compounds. The dipole moment was predicted for each of these conformations employing the bond-moment method.[19] The dipole moment must lie along the two-fold symmetry axis which will be present for all conformations of the molecule. This two-fold axis will be the *b* axis for dihedral angles less than about 106° from the *syn* position, and the *c* axis for angles in the ±106°–180° range, because, at about 106°, the molecule becomes an accidental symmetrical top.

A rotation of 180° about the two-fold axis of symmetry exchanges two pairs of bosons (the carbon atoms with spin =0) and three pairs of fermions (the two pairs of hydrogen atoms and the one pair of fluorine atoms, all with spins =½). The wave function must change sign for this operation. For a *b* type spectrum, it is found that the lines following the K_{-1},K_{+1} selection rule of the *ee*↔*oo* type will have a statistical weight of 28, and those following the *eo*↔*oe* selection rule will have a statistical weight of 36 according to Ref. 20.

Table 3. Selected transitions of the ground vibrational state of CH_2F-C≡C-CH_2F.

Transition	Observed frequency[a] (MHz)	Obs.-calc. frequency (MHz)	Centrifugal distortion	
			Total (MHz)	Sextic (MHz)
Q-branch				
$1_{1,0} \leftarrow 1_{0,1}$	13628.07	−0.17	−0.60	
$4_{1,3} \leftarrow 4_{0,4}$	13668.10	0.08	−0.48	
$9_{1,8} \leftarrow 9_{0,9}$	13823.04	−0.13	−0.41	
$15_{1,14} \leftarrow 15_{0,15}$	14158.05	0.21	−2.43	
$25_{1,24} \leftarrow 25_{0,25}$	15087.02	0.05	−23.90	0.02
$35_{1,34} \leftarrow 35_{0,35}$	16502.47	0.16	−103.37	0.45
$45_{1,44} \leftarrow 45_{0,45}$	18425.42	−0.09	−307.02	2.61
$55_{1,54} \leftarrow 55_{0,55}$	20858.33	−0.13	−733.23	10.05
$65_{1,64} \leftarrow 65_{0,65}$	23766.22	−0.09	−1510.35	30.25
$87_{1,86} \leftarrow 87_{0,87}$	31360.78	−0.01	−5198.44	198.11
$94_{1,93} \leftarrow 94_{0,94}$	33926.97	0.13	−7150.73	322.88
$101_{1,100} \leftarrow 101_{0,101}$	36458.88	−0.27	−9575.98	506.17
$42_{2,40} \leftarrow 42_{1,41}$	37713.51	0.10	189.07	−2.55
$50_{2,48} \leftarrow 50_{1,49}$	36779.34	0.12	279.70	−5.40
$61_{2,59} \leftarrow 61_{1,60}$	35597.94	0.16	374.27	−11.77
$70_{2,68} \leftarrow 70_{1,69}$	34800.32	−0.17	357.39	−18.08
$80_{2,78} \leftarrow 80_{1,79}$	34136.89	−0.10	137.71	−22.39
$91_{2,89} \leftarrow 91_{1,90}$	33662.11	−0.29	−489.93	−13.84
$100_{2,98} \leftarrow 100_{1,99}$	33415.59	−0.10	−1401.36	16.08
$108_{2,106} \leftarrow 108_{1,107}$	33238.54	0.02	−2579.67	72.17
$117_{2,115} \leftarrow 117_{1,116}$	33002.65	−0.05	−4351.88	183.67
$124_{2,122} \leftarrow 124_{1,123}$	32731.48	−0.03	−6052.81	316.17
R-branch				
$3_{1,12} \leftarrow 2_{0,2}$	20736.60	−0.20	−0.33	
$12_{0,12} \leftarrow 11_{1,11}$	15213.38	0.00	−5.58	
$23_{1,22} \leftarrow 22_{2,21}$	15014.07	−0.07	−54.37	0.15
$34_{2,32} \leftarrow 33_{3,31}$	12848.33	−0.58[b]	−120.32	0.88
$36_{2,34} \leftarrow 35_{3,33}$	17624.93	−0.63[b]	−148.56	1.13
$44_{2,43} \leftarrow 43_{3,40}$	36254.85	0.86[b]	−130.56	1.76
$57_{4,54} \leftarrow 56_{5,51}$	12659.17	0.11	−417.02	11.01
Coalescing K_{-1} doublet lines[c]				
$69_5 \leftarrow 68_6$	13664.28	0.08	−728.14	28.84
$79_5 \leftarrow 78_6$	37068.55	0.14	−1156.75	50.45
$90_6 \leftarrow 89_7$	35489.95	0.04	−1658.59	99.85
$101_7 \leftarrow 100_8$	33803.05	−0.38	−2268.01	181.91
$108_8 \leftarrow 107_9$	22836.83	0.03	−2627.53	267.42
$113_8 \leftarrow 112_9$	34297.32	0.08	−3076.72	322.18
P-branch				
$7_{2,5} \leftarrow 8_{1,8}$	21987.75	0.06	−7.11	
$19_{3,16} \leftarrow 20_{2,19}$	20531.58	−0.01	−4.89	−0.08
$29_{4,25} \leftarrow 30_{3,28}$	23983.52	0.02	13.13	−0.61
Coalescing K_{-1} doublet lines[c]				
$41_5 \leftarrow 42_4$	22741.95	0.08	86.27	−3.07
$58_7 \leftarrow 59_6$	36890.41	−0.06	194.75	−17.17
$78_8 \leftarrow 79_7$	17168.97	0.00	835.68	−65.69
$95_{10} \leftarrow 96_9$	31658.30	0.10	1277.92	−180.01

[a] ±0.10 MHz. [b] $K_{-1} = 3 \leftarrow 2$ transition which fits poorly. See text. [c] The K_{-1}-energy doublets coalesce for high J and K_{-1} quantum numbers.

In the theoretical calculation,[11] a dihedral angle of about 103° was found for the energy minimum. A strong *b* type *Q*-branch $J_{1,J-1} \leftarrow J_{0,J}$ series was thus predicted to start somewhere in the 13–16 GHz spectral region and spread out towards higher frequencies. Every other line should be of the *ee*↔*oo* type with weight 28, and every other of the *eo*↔*oe* species with weight 36.

This spectral feature was soon recognized and led to the assignment of *Q*-branch series and the numerous and strong $J_{2,J-2} \leftarrow J_{1,J-1}$ *Q*-branch transitions occurring in the upper *R*-band. The assignments were ultimately extended to very high values of *J* as shown in Table 3. This table also includes the *R*- and *P*-branch transitions which are scattered all over the spectrum, but are generally much less intense than the predominating *Q*-branch lines. The first $\Delta J = 1$ transitions found belonged to the $J+1_{0,J+1} \leftarrow J_{1,J}$ series. A trial and error procedure was used to identify these lines. Extension to further series of *P*- and *R*-branch lines was rather easy. No ground state lines were split.*

The assymetry parameter,[21] κ, was found to be approximately −0.999. Initially, the spectrum was fitted to Watson's *A*-reduction *I*ʳ-representation[22] Hamiltonian, but a satisfactory fit could only be obtained with this procedure for rather low or intermediate values of *J*. This difficulty is often encountered for the *A*-reduction for asymmetric molecules which are close to a symmetrical top, as already discussed in the literature.[23]

Our final choice of Hamiltonian analysis was the one suggested by Sørensen.[24] With this procedure, τ_{aaaa}, τ_{bbbb}, τ_{cccc}, $D_4 = T_4 + ((A-B)/(A-C))T_6$, and $D_5 = T_5 + ((B-C)/(A-C))T_6$ are chosen as the five quartic centrifugal distortion constants which can be determined. T_4, T_5 and T_6 are defined in Ref. 24. Since high values of *J* were subsequently assigned, it was necessary to include sextic distortion constants in order to obtain a good fit. Attempts to determine all seven sextic constants simultaneously proved futile. It was found that only four of them, Φ_J, Φ_{JK}, φ_J, and φ_{JK} could be determined. In the final fit, the remaining three sextic constants were restricted to zero. With this procedure, about 340 ground state transitions were assigned, and 312 of them were used to determine the spectroscopic constants shown in Table 4. Transitions involving very high values of *J* were sufficiently strong to

*The complete spectral data of the ground as well as of the excited states are available from the authors upon request or from the Molecular Data Spectra Center. Molecular Spectroscopy Division, National Bureau of Standards, B268 Physics Building, Gaithersburg, MD 20899, USA.

Table 4. Spectroscopic constants[a] for $CH_2F\text{-}C{\equiv}C\text{-}CH_2F$.

Vibrational state	Ground	First ex. torsion[b]	First ex. second lowest bending
Number of transitions	312	114	40
R.m.s.[c]/MHz	0.134	0.321	0.208
A/MHz	14818.285(12)	14860.039(65)	14939.64(13)
B/MHz	1194.2533(10)	1194.6913(52)	1191.4362(44)
C/MHz	1185.4504(10)	1186.1606(53)	1183.6900(66)
τ_{aaaa}/MHz	−2.38802(38)	−2.4463(39)	*f*
τ_{bbbb}/MHz	−0.00168603(96)	−0.001758(11)	−0.0018955(15)
τ_{cccc}/MHz	−0.00069519(96)	−0.000660(11)	*f*
D_J^g/MHz	−0.042350(14)	−0.04924(18)	−0.0212(10)
D_{JK}^g/MHz	0.00014731(5)	0.0001920(14)	0.0002258(86)
Φ_J^g/Hz	−0.000398(23)	−0.00118(41)	*f*
Φ_{JK}/Hz	−0.1515(10)	−0.177(16)	*f*
φ_J/Hz	0.00029960(39)	0.000369(19)	*f*
φ_{JK}/Hz	0.00004886(33)	0.000177(30)	*f*

[a]Uncertainties represent one standard deviation. [b]Derived from average frequencies; see text. [c]Root-mean-square deviation. [d]Distortion constants defined by Sørensen;[24] see text. [e]Further sextic constants present at zero. [f]Kept at ground state value.

Table 5. Selected transitions of the first excited torsional state of CH_2F-C≡C-CH_2F.

Transition	ν_H^a	ν_H-ν_L^b	$\bar{\nu}^c$	$\Delta\bar{\nu}^d$	Centrifugal distortion	
	(MHz)	(MHz)	(MHz)	(MHz)	Total (MHz)	Sextic (MHz)
Q-branch						
$16_{1,15} \leftarrow 16_{0,16}$	14255.48	0.99	14254.99	*0.06*	*−3.98*	*−0.01*
$25_{1,24} \leftarrow 25_{0,25}$	15080.99	0.32	15080.83	*−0.03*	*−27.38*	*0.03*
$32_{1,31} \leftarrow 32_{0,32}$	15980.70	0.73	15980.34	*0.04*	*−78.91*	*0.28*
$37_{1,36} \leftarrow 37_{0,37}$	16763.84	0.97	16763.36	*−0.12*	*−146.92*	*0.82*
$41_{1,40} \leftarrow 41_{0,41}$	17475.52	1.21	17474.92	*−0.08*	*−228.16*	*1.68*
$47_{1,46} \leftarrow 47_{0,47}$	18683.34	1.17	18682.76	*0.08*	*−410.32*	*4.26*
$55_{1,54} \leftarrow 54_{0,54}$	20546.10	1.04	20545.63	*−0.01*	*−807.48*	*12.10*
$63_{1,62} \leftarrow 63_{0,63}$	22672.00	1.44	22671.28	*−0.07*	*−1448.60*	*29.45*
$66_{1,65} \leftarrow 66_{0,66}$	23528.02	1.16	23527.44	*0.09*	*−1768.60*	*39.84*
$57_{2,55} \leftarrow 57_{1,56}$	36264.30	1.10	36263.75	*0.09*	*381.99*	*−9.09*
$61_{2,59} \leftarrow 61_{1,60}$			36853.54[e]	*−0.05*	*406.90*	*−10.77*
$65_{2,63} \leftarrow 65_{1,64}$			35467.68[e]	*0.37*	*428.03*	*−13.53*
$69_{2,67} \leftarrow 69_{1,68}$	35110.50	1.24	*35109.88*	*−0.61*	*419.41*	*−15.35*
R-branch						
$9_{1,9} \leftarrow 8_{0,8}$			34907.23[e]			
$14_{0,14} \leftarrow 13_{1,13}$			20035.55[e]	0.53	−9.50	
$24_{1,23} \leftarrow 23_{2,22}$			17336.81[e]	0.52	−68.15	0.20
$38_{2,37} \leftarrow 37_{3,34}$	21929.92	0.94	21929.45	0.20	−91.53	0.75
$59_{4,56} \leftarrow 58_{5,53}$			17006.45[e]	0.04	−493.43	12.36
Coalescing lines[f]						
$60_4 \leftarrow 59_5$			19361.32[e]	0.10	−523.17	13.21
$69_5 \leftarrow 68_6$			13208.25[e]	0.07	−758.65	28.29
$73_5 \leftarrow 72_6$			22575.58[e]	−0.37	−926.88	35.36
P-branch						
$20_{3,18} \leftarrow 21_{2,19}$			18330.84[e]	−0.30	6.85	−0.12
$21_{3,18} \leftarrow 22_{2,21}$			15983.92[e]	−0.40	3.49	−0.12
Coalescing lines[f]						
$30_4 \leftarrow 31_3$			21895.97[e]	0.13	26.55	−0.72
$44_5 \leftarrow 45_4$	16018.75	0.40	16018.55	−0.10	150.53	−4.16
$55_6 \leftarrow 56_5$	17315.54	0.96	17315.07[e]	−0.18	301.75	−12.22
$57_6 \leftarrow 58_5$			12612.20[e]	0.35	363.52	−14.10
$77_8 \leftarrow 78_7$			20134.70[e]	−0.02	827.93	−62.83

[a]ν_H is high frequency component. ν_L is low frequency component. Accuracy is ±0.15 MHz for each of these components. [b]High frequency minus low frequency splitting. [c]Average frequency. [d]Difference between average frequency of previous column and the value calculated using the spectroscopic constants of Table 4. [e]No splitting resolved. [f]Comments as for [c]of Table 3.

be assigned. The maximum J value was 124 for the Q-branch transitions, 113 for R- and 96 for P-branch lines as shown in Table 3. Very accurate quartic as well as sextic constants were obtained (Table 4). In fitting these transitions, one difficulty was seen. For the relatively strong R-branch $K_{-1}=2\leftarrow3$ series with J between 33 and 43, deviations between approximately 0.3 MHz and 0.8 MHz from predicted frequencies were found in most cases. Whether this was due to inadequacy

of the Hamiltonian method employed or to resonances with, for example, the low lying vibrational torsional levels, is difficult to say.

The dipole moment was of interest, and the Stark effect of many low J transitions was studied in an attempt to determine it. Unfortunately, these transitions were so weak that no quantitative measurements could be made, hence, no dipole moment was determined.

Vibrationally excited states. One prominent excited state was assigned simultaneously with the ground state. Most of its lines were split into two components of apparently equal intensities. These splittings were all less than about 1.5 MHz, and are presumed to result from low barrier tunnelling. Selected transitions are displayed in Table 5. Relative intensity measurements using integrated intensities performed as described in Ref. 25 yielded 67(30) cm^{-1} for this vibrational mode: this is certainly the torsional vibration. This torsional frequency is in fair agreement with 30–40 cm^{-1} seen in the IR gas spectrum, as mentioned above. The average frequencies of the two split components were used to derive the spectroscopic constants listed in Table 4; the maximum value of J was 78. The first excited state of the second lowest bending mode was also found, as shown in Table 4. None of its lines were split, and the intensities were about 30 percent of the corresponding ground state transitions. Relative intensity measurements[25] yielded 188(40) cm^{-1} in agreement with *ca.* 150 cm^{-1} from the IR vapour spectrum.

The assignments reported above include all the strongest as well as the majority of the intermediate intensity transitions present in the microwave spectrum. However, there remains a very large number of lines which were not assigned. According to the potential function (see below), there are several low lying torsional excited states which will be rather well populated at −40 °C. Coupling between vibration/torsion and rotation resulting in nonrigid rotor behavior is expected for these excited states, and may be the reason why assignments could not be made despite numerous trials.

The second excited torsional state should be situated at ca. 80 cm^{-1} above the vibrational ground state. It should thus be quite intense. Searches for this excited state were made, but it was not found. We believe the reason for this is extensive tunnelling.

There are two heavy atom bending modes as discussed above. Searches for the microwave transitions belonging to the first excited state of the lower one of these two bending modes were unsuccessful. We believe that this state at ca. 120 cm^{-1} is strongly perturbed by the third excited state of the torsional mode.

Potential function. The torsional potential function was assumed to depend only on the dihedral angle φ and to be approximated by

$$V(\varphi) = \tfrac{1}{2}\Sigma V_i(1-\cos(i\varphi)).$$

It is unlikely that terms above V_2 are large.[11] Higher terms were therefore neglected and we have for $\varphi = 99^{10}$

$$\frac{dV(\varphi)}{d\varphi} = 0$$

and

$$\frac{d^2V(\varphi)}{d\varphi^2} = 4\pi^2\nu^2G_{tt}^{-1}.$$

G_{tt}^{-1} represents the diagonal element of the torsion of the G^{-1} matrix. Its value was found to be 9.65 $um^2 \times 10^{-20}$ by inverting the G matrix. ν is the harmonic torsional frequency which was determined in three independent ways. From microwave intensity data, the rather inaccurate value of 67(30) cm^{-1} was obtained as described above. In the gas phase IR spectrum, a strong band between 30 and 40 cm^{-1} was assigned as this mode (see above). However, in our opinion, a slightly better value for ν can be obtained from the quartic centrifugal distortion constants in the way described in Ref. 26. By using these constants in a least squares fit, keeping all force constants fixed except the torsional, a frequency of 42 cm^{-1} was calculated (see Table 2). A liberal uncertainty limit is 5 cm^{-1}. The two first potential constants are then found as $V_1 = -1.9(4)$ kJ mol^{-1}, and $V_2 = -3.1(7)$ kJ mol^{-1}. The uncertainties are estimated to be about three standard deviations. These potential constants are rather similar to $V_1 = -3.25$ kJ mol^{-1} and $V_2 = -3.50$ kJ mol^{-1} found by Radom *et al.*[11]

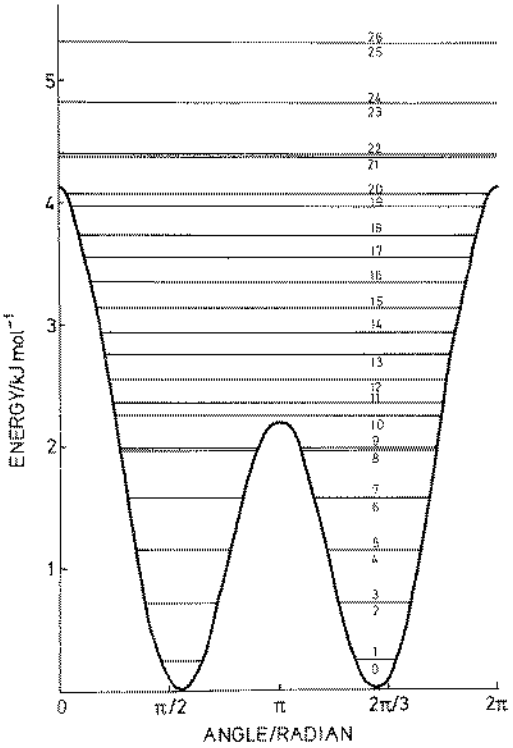

Fig. 9. Torsional potential function of CH_2-F-C≡C-CH_2-F with its 26 lowest torsional levels calculated using $V_1 = -1.9$ kJ mol^{-1} and $V_2 = -3.1$ kJ mol^{-1} and $B_0 = 1.76$ cm^{-1}.

Using these potential constants, the barrier at *syn* was calculated to be 4.1(10) kJ mol^{-1} and the barrier at *anti* to be 2.2(5) kJ mol^{-1}, very close to 5.33 kJ mol^{-1} and 3.23 kJ mol^{-1}, respectively, found by the theoreticians.[11] The potential function is drawn in Fig. 9. The 26 lowest torsional levels indicated in this figure were calculated employing the procedure of Lewis *et al.*[27] using a program written by Bjørseth.[28] Only the B_0 of Ref. 27 was utilized, and its value was calculated to be 1.76 cm^{-1}.

Structure. Only three rotational constants were determined for the title compound. Hence, a full structure cannot be calculated. Several assumptions have to be made. The plausible structural parameters appearing in Table 6 were taken from recent, accurate studies of related compounds. The carbon atoms were assumed to be linear. The dihedral angle was varied in steps of 1°, the C-F bond length in steps of 0.5 pm, and the C-C-F angle in steps of 0.2°. These structural parameters were chosen because they are chemically interesting and because the rotational constants are very sensitive to them. The results of this fit are shown in Table 6, and the uncertainties quoted there are estimated to be about three standard deviations.

The F-C-C≡C-C-F dihedral angle of 99(3)° from *syn* (81(3)° from *anti*) shown in this table compares well with 103.7° found in the theore-

Table 6. Plausible structural parameters[a] (bond lengths in *pm*; angles in *degrees*) of CH_2F-C≡C-CH_2F.

Assumed structural parameters kept fixed			
C≡C	120.6	∠C-C-H	109.47
C–C	146.0		
C–H	109.3		
Fitted structural parameters[b]			
C–F	138(1)	∠F-C-C≡C-C-F[c]	99(3)°
		∠C-C-F	111.5(10)°
Rotational constants/MHz			
	Obs.	Calc.	Diff. (%)
A	14814.29	14830.16	0.10
B	1194.25	1193.23	0.08
C	1185.45	1185.01	0.04

[a]See text. [b]Uncertainties are estimated to be about three standard deviations. [c]Dihedral angle measured from *syn*.

tical work.[11] The C-F bond length was determined to be 138(1) pm and the C-C-F angle was found as 111.5(10)°. These values are very similar to 139.3(6) pm and 111.0(4)°, respectively, determined in a very recent study of the related molecule H-C≡C-CH_2-F.[39]

Acknowledgement. The authors wish to thank Dr. H. Priebe for his valuable suggestions for the synthesis of the title compound.
Financial support from the Nansen Foundation is also acknowledged.

References

1. Bak, B., Christiansen, J. J. and Madsen, E. *Acta Chem. Scand. 14* (1960) 573, and papers listed there.
2. Dellepiane, G. D. and Gussoni, M. *J. Mol. Spectrosc. 47* (1978) 515.
3. Lichene, F., Dellepiane, G. and Lorenzelli, V. *J. Chem. Phys. 70* (1979) 4786.
4. Crowder, G. A. *J. Mol. Struct. 12* (1974) 302.
5. Ellestad, O. H. and Kveseth, K. *J. Mol. Struct. 25* (1975) 175.
6. Sipos, P. A. and Phibbs, M. K. *Can. J. Spectrosc. 21* (1976) 69.
7. Mannik, L., Sipos, P. A. and Phibbs, M. K. *Can. J. Spectrosc. 21* (1976) 105.
8. Suzuki, S. *J. Mol. Struct. 46* (1978) 155.
9. Kuchitsu, K. *Bull. Chem. Soc. Jpn. 30* (1957), 391, 399.
10. Kveseth, K., Seip, H. M. and Stølevik, R. *Acta Chem. Scand. 25* (1971) 13.
11. Radom, L., Stiles, P. J. and Vincent, M. A. *J. Mol. Struct. 48* (1978) 259.
12. Karlsson, A., Klæboe, P. and Nielsen, C. J. *To be published.*
13. Pattison, F. L. H. and Norman, J. J. *J. Am. Chem. Soc. 79* (1957) 2311.
14. Bunker, P. R. *Molecular Symmetry and Spectroscopy,* Academic Press, London 1979.
15. Evans, J. C. and Nyquist, R. A. *Spectrochim. Acta 19* (1963) 1153.
16. Kopelman, J. *J. Chem. Phys. 41* (1964) 1547.
17. Nielsen, C. J. *Spectrochim. Acta 39A* (1983) 993.
18. Klæboe, P. *Zeitschr. Chem. (Leipzig) 21* (1981) 381.
19. Smyth, C. P. *Dielectric Behavior and Structure,* McGraw-Hill, New York 1955, p. 244.
20. Gordy, W. and Cook, R. L. *Microwave Molecular Spectra,* Wiley, New York 1984, p. 61.
21. *Ibid.* p. 229.
22. *Ibid.* p. 324.
23. *Ibid.* p. 333.
24. Sørensen, G. O. *J. Mol. Spectrosc. 22* (1967) 325.
25. Esbitt, A. S. and Wilson, E. B., Jr. *Rev. Sci. Instrum. 34* (1963) 901.
26. Braathen, O. A., Marstokk, K.-M. and Møllendal, H. *Acta Chem. Scand. A36* (1982) 173.
27. Lewis, J. D., Malloy, Jr., T. B., Chao, T. H. and Laane, J. *J. Mol. Struct. 12* (1972) 427.
28. Bjørseth, A. *Personal communication.*
29. Wiedenmann, K.-H., Botskor, I. and Rudolph, H.-D. *J. Mol. Spectrosc. 113* (1985) 186.

Received February 3, 1986.